Variable Range Hopping and Thermal Activation Conduction of Y-doped ZnO Nanocrystalline Films

T. T. Lin[a], S. L. Young[b,*], C. Y. Kung[a,*], H. Z. Chen[b], M. C. Kao[b], M. C. Chang[a], C. R. Ou[c]
[a]Department of Electrical Engineering, National Chung Hsing University, Taichung, Taiwan
[b]Department of Electronic Engineering, Hsiuping University of Technology, Taichung, Taiwan
[c]Department of Electrical Engineering, Hsiuping University of Technology, Taichung, Taiwan
Phone: (+886) 4-24961100ext1206, E-mail: slyoung@mail.hust.edu.tw and cykung@nchu.edu.tw

Abstract

ZnO and Y-doped ZnO nanocrystalline films were separately fabricated on the glass substrates by sol-gel spin-coating method. X-ray diffraction patterns of the films show the same wurtzite hexagonal structure and (002) preferential orientation. SEM images show that grain size and thickness of the nanocrystalline films decrease with increasing doping concentration. The decrease of optical bandgap with the increase of Y doping is deduced from the transmittance spectra. Temperature-dependent resistivity reveals a semiconductor transport behavior for all ZnO and Y-doped ZnO nanocrystalline films. The resulting conductivity originates from the combination of thermal activation conduction and Mott variable range hopping (VRH) conduction. In the high temperature range, the temperature-dependent resistivity can be described by the Arrhenius equation, $\sigma(T)=\sigma_0 exp[-(E_a/kT)]$, which shows the thermal activation conduction. The activation energy E_a increases from 0.47 meV for ZnO film to 0.83 meV for $Zn_{0.98}Y_{0.02}O$ film. On the contrary, in the low temperature range, the temperature-dependent resistivity can be fitted well by the relationship, $\sigma(T)=\sigma_{h0} exp[-(T_0/T)^{1/4}]$, which indicates the behavior of Mott VRH. The results demonstrate that the crystallization and the corresponding carrier transport behavior of the ZnO and Y-doped ZnO nanocrystalline films are affected by Y doping.

Keywords: ZnO nanocrystalline film, sol-gel spin-coating method, resistivity, variable range hopping, thermal activation conduction.

Introduction

Recently, a great deal of exertions has been directed toward zinc oxide (ZnO) researches for the possible application in optoelectronics devices [1-3]. Due to the large direct bandgap (3.37 eV) and exciton energy (60 meV), the optical and electronic properties of ZnO are important to commercial products, such as photoconductors for electrophotography [4], varistors for electrical circuits [5], sensors for gas detection [6], and active layer for thin film transistors [7]. In addition, there are also optical transparent ZnO films with high conductivity, which are candidates for transparent electrodes in solar cell and liquid crystal display applications [8, 9].

Magnetic doped ZnO has attracted broad interests for their possible use as spintronic materials [10-11]. ZnO doped with transitional magnetic metal, such as $Zn_{1-x}TM_xO$ (TM=Mn, Fe, Co, and Ni) [12-15] were found to be diluted magnetic semiconductors with high Curie temperature. Some previous researchers reported that the inhomogeneous distribution of transitional metal might greatly influence the magnetic and electronic properties of the ZnO-based materials [16-18].

The ZnO-based thin films have been investigated through various kinds of fabrication methods, such as sputtering, pulsed laser deposition, chemical vapor deposition, spray pyrolysis, sol-gel method, etc. However, compared with these higher vacuum fabrication procedures, solution-based processes (spray pyrolysis and sol-gel methods) offer more merits dut to ease-control of chemical composition and much simpler method for large area coating at a low cost. ZnO thin films prepared by spray pyrolysis and their corresponding electrical characterization had been well studied [19], while the optical properties of doped ZnO thin films deposited by sol-gel method had also been reported [20-21]. Therefore, it becomes critical to investigate the carrier transport behavior of the ZnO-based films.

The temperature-dependent resistivity contains a wealth of information on the electronic and lattice states [22], while various electrical transport models, thermal activation conduction in the high temperature range and variable-range hopping (VRH) conduction in the low temperature range, had been reported to clarify the mechanism of the temperature-dependent conduction for the non-crystalline materials [23]. Transformation of conduction mechanism for doped ZnO compounds has progressively studied by changing density of states (DOS) with structural modulation [24-25]. The temperature-dependent resistivity for ZnO-based films can also be controlled by the fabrication process, which is mainly due to zinc excess at interstitial position. In the present investigation, we will concentrate on the variances of the structural and electrical characteristics caused by Y doping in the transparent ZnO nanocrystalline films. At the same time, the report will also discuss on the temperature dependence of carrier transport mechanisms in various temperature ranges, as a guiding rule for possible application.

Experimental Procedure

The $Zn_{1-x}Y_xO$ (x=0, 0.005, 0.01, and 0.02) nanocrystalline

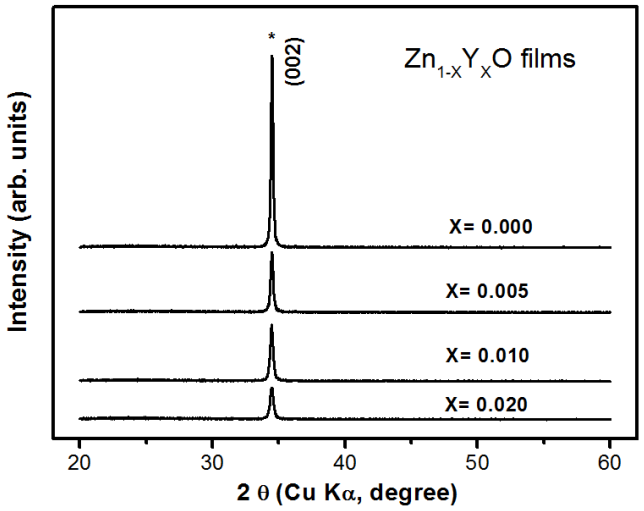

Fig. 1 X-ray diffraction patterns of $Zn_{1-x}Y_xO$ nanocrystalline films grown on glass substrates.

films were deposited on the glass substrates by sol-gel spin coating method. The source solutions were separately prepared by $Zn(C_2H_3O_2)_2{\cdot}2H_2O$ (zinc acetate dehydrate), $Y(C_2H_3O_2)_3{\cdot}4H_2O$ (yttrium acetate tetrahydrate), $C_3H_8O_2$ (2-methoxyethanol), and C_2H_7NO (MEA, ethanolamine). The metal ionic sources, zinc acetate dehydrate and yttrium acetate tetrahydrate, were firstly dissolved in 2-methoxyethanol in stoichiometric proportions. The concentration of metal ions was kept at 0.5 M with yttrium mole ratios of 0, 0.5, 1, and 2%, respectively. Later, MEA was added into the solutions to form stable precursor solutions. The molar ratio of MEA to the combination of zinc acetate dehydrate and yttrium acetate tetrahydrate was kept at 1:1 for all solutions. The solutions were separately stirred at 150°C on a hot-plate for 1 h using a magnetic stirrer to get transparent sols, which served as the coating sols after being kept still for 3 days. $Zn_{1-x}Y_xO$ thin films were separately deposited on glass substrates by spin coating technique with the coating sols. The sols were dropped on the glass substrates and spun at 2500 rpm for 30 sec. In the final stage, the samples were annealed by rapid thermal annealing treatment in air at 800°C for 2 min with a heating rate of 600°C/min.

The crystal structure and grain orientation of ZnO films were determined by the x-ray diffraction (XRD) patterns using a Rigaku D/max 2200 x-ray diffractometer with Cu-Kα radiation. The XRD data were recorded at room temperature under the 2θ range from 20° to 60° with a step width of 0.01° and a scan speed of 0.5°/min. Morphological characterization was examined using a field emission scanning electron microscope (FE-SEM, JEOL JSM-6700F) at 3.0 kV. Energy dispersive spectroscopy (EDS) was utilized to analyze the chemical composition of $Zn_{1-x}Y_xO$ films by the energy dispersive X-ray spectrometer (Oxford Instruments INCA). Eventually, four-probe resistivity measurement was carried out using a Keithley Model 2400 sourcemeter. The samples were mounted on the sample holder which was situated inside a stainless vacuum container in an Oxford gas helium cooled cryostat system.

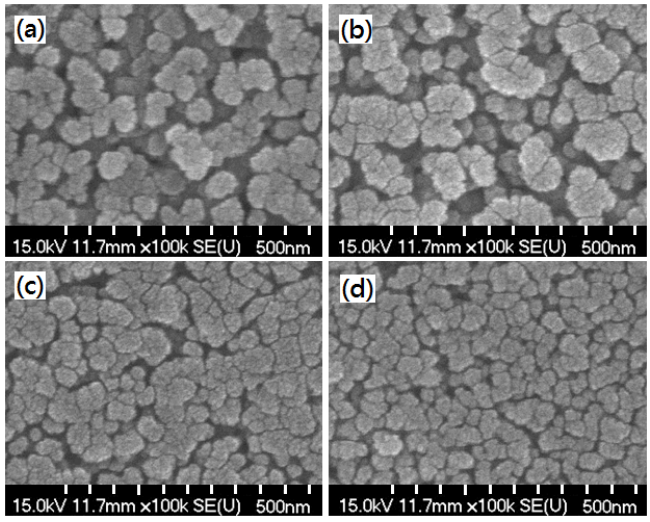

Fig. 2 SEM surface images of (a) ZnO, (b) $Zn_{0.995}Y_{0.005}O$, (c) $Zn_{0.99}Y_{0.01}O$ and (d) $Zn_{0.98}Y_{0.02}O$ nanocrystalline films grown on glass substrates.

Results and Dissusion

Fig. 1 illustrates the XRD patterns of all $Zn_{1-x}Y_xO$ nanocrystalline films. As shown from the XRD patterns, all Y-doped ZnO samples are found to have a single polycrystalline phase with the same wurtzite hexagonal crystal structure of space group $P6_3/mc$ (JCPDS 36-1451) as undoped ZnO film, and there is no omen of the secondary phase. The entire compositions exhibit the conspicuous (002) diffraction peak at about $2\theta = 34.5°$, which indicates *c*-axis preferential orientation. The decreasing of the (002) diffraction peak intensity shows that the crystallization is restrained by the doping of Y in the ZnO film. Moreover, a gradual increasing of the half maximum at full wavelength of the (002) diffraction peak from ZnO to $Zn_{0.98}Y_{0.02}O$ sample can be explained as the decreasing of the grain sizes. The average grain sizes of the samples calculated by the classical Scherrer formula are 48.3 nm, 41.2 nm, 34.3nm, and 28.4 nm for x=0, 0.005, 0.01, and 0.02 of $Zn_{1-x}Y_xO$ nanocrystalline films, respectively. The decreasing of grain size with Y doping in the ZnO film leads to the raising of boundary to volume ratio. In this report, the predictable increasing of resistivity with Y doping is verified by the following measurement of the temperature-dependent resistivity.

Fig. 2 shows the FE-SEM surface images of $Zn_{1-x}Y_xO$ nanocrystalline films that reveal porous and granular morphology for all samples. It is noted that the grain size of the $Zn_{0.98}Y_{0.02}O$ film is proving to be smaller than that of the ZnO film, which is consistent with the predictions from the XRD patterns. Besides, the thickness of the $Zn_{1-x}Y_xO$ films also gradually decreases from 242, 225, 205 to162 nm for x=0, 0.005, 0.01, and 0.02 of $Zn_{1-x}Y_xO$ nanocrystalline films, respectively.

To determine the dominant compositions of $Zn_{1-x}Y_xO$ nanocrystalline films, EDS spectra were measured as shown in Fig. 3. These peak positions denoted as O–Kα, Zn–Lα, Y–Kα,

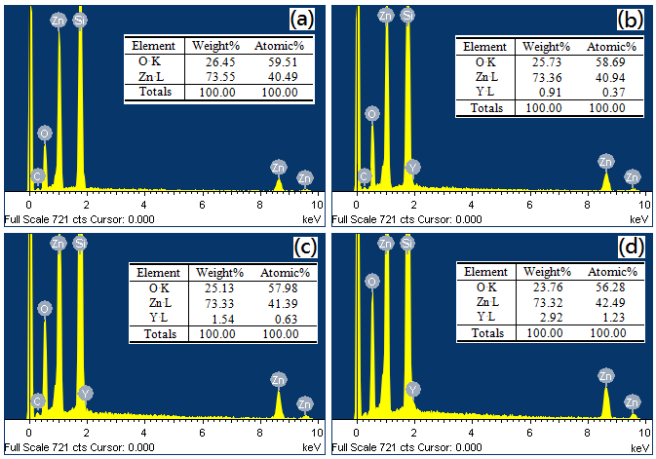

Fig. 3 EDS spectra of (a) ZnO, (b) $Zn_{0.995}Y_{0.005}O$, (c) $Zn_{0.99}Y_{0.01}O$ and (d) $Zn_{0.98}Y_{0.02}O$ nanocrystalline films grown on glass substrates.

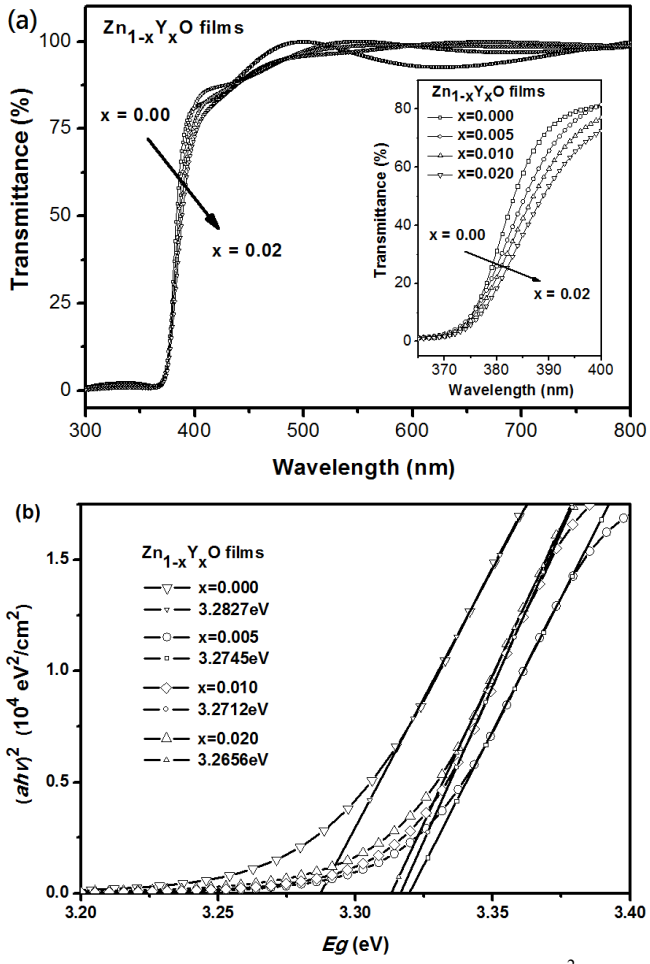

Fig. 4 (a) Optical transmittance and (b) Plot of $(\alpha hv)^2$ versus E_g of $Zn_{1-x}Y_xO$ nanocrystalline films.

Y–Kβ, Zn–Kα, and Zn–Kβ are appeared at 0.525, 1.012, 1.922, 2.000, 8.630, and 9.572 keV, respectively. Additional peaks at 0.277 and 1.740 keV denoted as C–Kα and Si–Lα are resulted from the conductive tape and substrate, respectively. The contents of Y dopant in the $Zn_{1-x}Y_xO$ nanocrystalline films

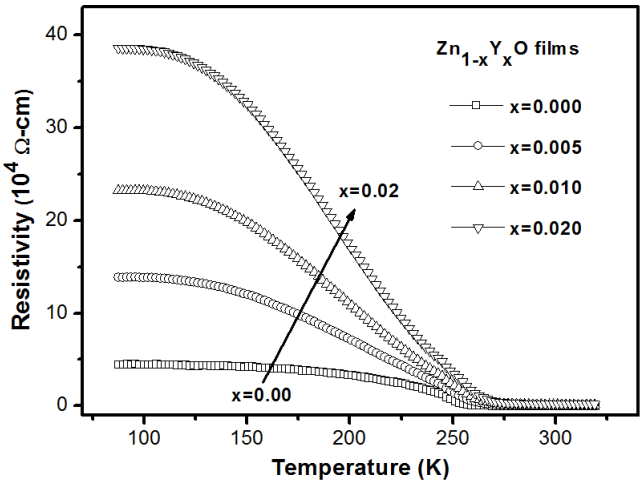

Fig. 5 Temperature-dependent resistivity of $Zn_{1-x}Y_xO$ nanocrystalline films.

examined by the EDS results show that the Y atomic percentages were 0, 0.37, 0.63, and 1.23% for x= 0, 0.005, 0.01, and 0.02, respectively. The results also reveal the effective doping of Y into $Zn_{1-x}Y_xO$ films.

Fig. 4(a) gives the transmittance spectra of $Zn_{1-x}Y_xO$ nanocrystalline films within the wavelength range from 300 to 800 nm. As shown in Fig. 4(a), the $Zn_{0.98}Y_{0.02}O$ film reveals a slightly degrades of transmission by the doping of Y in the ZnO films. Speculation for this is the increasing of possible defects and grain boundary to volume ratio that caused by the decreasing of the grain size. Optical spectra are the most direct and perhaps simplest method for probing the band structure of semiconductors and the optical bandgap, *Eg*, can be calculated by the following relation [26]

$$\alpha = A(hv - E_g)^2/(hv), \quad (1)$$

where A is a constant. The details of the mathematical determination of the absorption coefficient α could be found in the literature [27]. Clearly, a progressive red shift as shown in Fig. 4(b) from ZnO to $Zn_{0.98}Y_{0.02}O$ films indicates the decrease of E_g. The estimated bandgaps deduced from the plots of $(\alpha hv)^2$ versus hv are 3.2827, 3.2745, 3.2712, and 3.2656 eV for x=0, 0.005, 0.01, and 0.02 of $Zn_{1-x}Y_xO$ nanocrystalline films, respectively. The tiny red shift of UV-Visible transition wavelength also indicates the increase of the defect-induced near-band-edge (NBE) transition which results in the bandgap narrowing.

For the temperature effects, Fig. 5 reveals the resistivity as functions of temperature from 75 to 320 K for the four representative $Zn_{1-x}Y_xO$ nanocrystalline films. The results show that the resistivity increases with decreasing temperature over the entire measured temperature range, which exhibits a typical semiconductor behavior in the electrical transport property. Besides, the resistivity of the $Zn_{0.98}Y_{0.02}O$ nanocrystalline film is obviously greater than that of ZnO nanocrystalline film which can be explained by the decrease of grain size and corresponding increase of grain boundary resistivity due to the Y doping in the films. In order to explore the mechanism for the carrier transport, the performance of the temperature-dependent resistivity will be separately

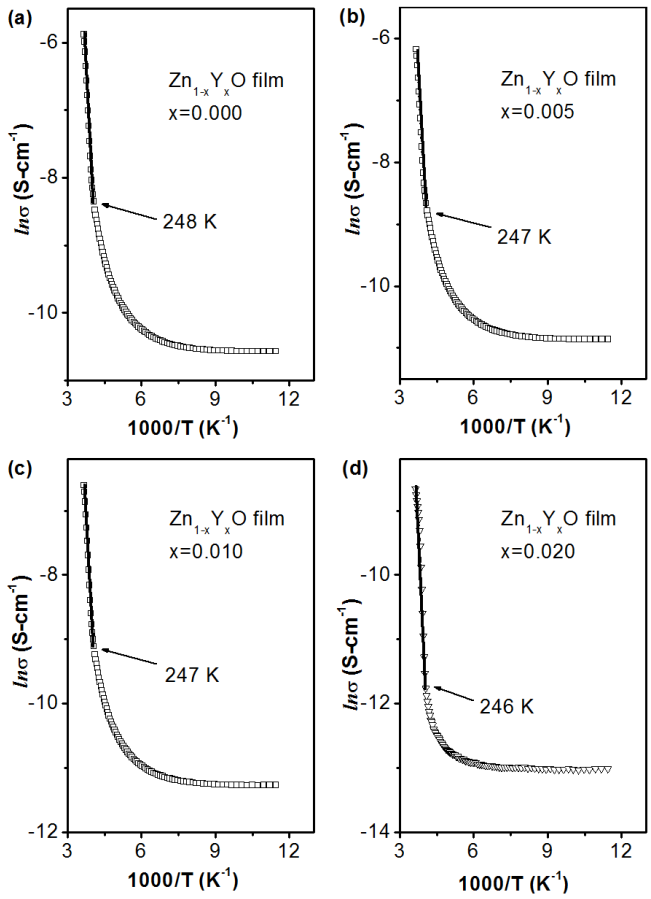

Fig. 6 Plots of $ln\sigma$ versus $1000/T$ of (a) ZnO, (b) $Zn_{0.995}Y_{0.005}O$, (c) $Zn_{0.99}Y_{0.01}O$ and (d) $Zn_{0.98}Y_{0.02}O$ nanocrystalline films measured in the high temperature range.

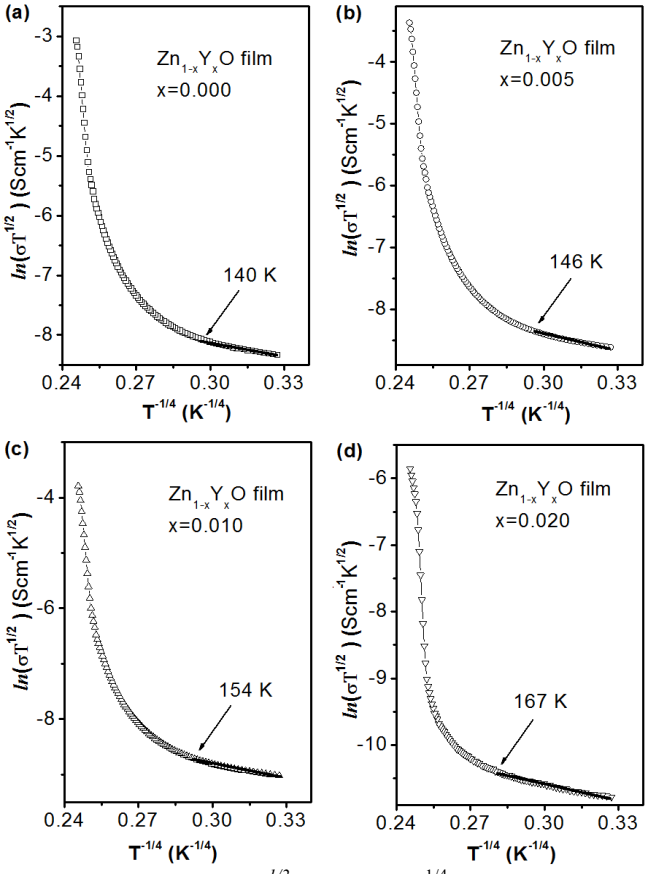

Fig. 7 Plots of $ln(\sigma T^{1/2})$ versus $T^{-1/4}$ of (a) ZnO, (b) $Zn_{0.995}Y_{0.005}O$, (c) $Zn_{0.99}Y_{0.01}O$ and (d) $Zn_{0.98}Y_{0.02}O$ nanocrystalline films measured in the low temperature range.

discussed in relatively high and low regions.

Through the examining on the carrier transport process in high temperature region, Fig. 6 gives the plots of all $Zn_{1-x}Y_xO$ nanocrystalline films fitted by the Arrhenius equation for thermal activation conduction measured in the high temperature region. The high temperature conduction process in semiconductor usually comes from the electrons hopping from the donor levels to the conduction band or from valence band to acceptor levels. The relationship of conductivity σ versus temperature T can be expressed as

$$\sigma(T)=\sigma_o \exp[-(E_a/kT)], \quad (2)$$

where σ_0 is a pre-exponential factor, E_a is the activation energy and k is the Boltzmann's constant. As shown in Fig. 6, experimental data on $Zn_{1-x}Y_xO$ nanocrystalline films can be fitted well by equation (2) in the temperature range higher than about 248 K. The activation energy of the $Zn_{1-x}Y_xO$ nanocrystalline films obtained from equation (2) is 0.47, 0.55, 0.67 and 0.83 meV for x=0, 0.005, 0.01, and 0.02, respectively. However, the conductivity deviates from the fitting line at lower temperature for all samples. Hence, the deviations from the fitted line with experimental data for all samples indicate the existence of different conduction mechanism in the lower temperature region.

As the temperatures goes down, a crossover to the hopping conduction process is observed. Eventually, in the relatively low temperature range, the temperature-dependent longitudinal conductivity by the variable-range hopping (VRH) model was described by the form, $ln\sigma(T)\propto(T_M/T)^n$, where n depends on the shape of the density of states (DOS) at the Fermi level [28]. For disordered systems without Coulomb interaction, the model of Mott variable range hopping conductivity, $ln\sigma\propto(T_M/T)^{1/4}$, was proposed based on the assuming that the DOS is a constant near the Fermi energy. For two-dimensional system, the variable range hopping mode, $ln\sigma\propto(T_{ES}/T)^{1/3}$, was proposed by Pollak and co-workers.[29]. For the existing of the Coulomb interaction between initial and final hopping sites [30], the Efros and Shklovskii variable range hopping mode, $ln\sigma\propto(T_{ES}/T)^{1/2}$, was proposed for long range electron-electron Coulomb interaction system in which DOS vanished quadratically at the Fermi level. The last mode of "hard gap" conductivity, $ln\sigma\propto(T_H/T)$, was observed in some systems with many-electron excitation effect which could lead to a hard gap in the density of state near Fermi level [31].

In the low temperature region, these four possible conduction mechanisms had been examined for carrier transport behavior of semiconductors. If any plot of $ln\sigma$ versus $T^{-1/4}$, $T^{-1/3}$ $T^{-1/2}$, or T^{-1} can be fitted well in low temperature region, it indicates the presence of an above particular hopping

model. However, all experimental data measured from $Zn_{1-x}Y_xO$ nanocrystalline films can only be fitted well by Mott VRH mode in the low temperature range. Hence, Mott VRH is the dominant conduction mechanism of $Zn_{1-x}Y_xO$ films in the present cases. For the Mott VRH conduction mechanism, the conductivity σ can be expressed as

$$\sigma(T)=\sigma_{h0}exp[-(T_0/T)^{1/4}], \quad (3)$$

where σ_{h0} and T_0 are given by the following expressions [32-33],

$$\sigma_{h0}=\frac{3e^2v_{ph}}{(8\pi)^{1/2}}\left[\frac{N(E_F)}{\alpha kT}\right]^{1/2}, \quad (4)$$

and

$$T_0=\left[\frac{16\alpha^3}{kN(E_F)}\right], \quad (5)$$

in which v_{ph} (about 1.7×10^{13} s^{-1}) is the phonon frequency at Debye temperature, k is the Boltzmann's constant, $N(E_F)$ is the density of state at Fermi level and α is the inverse localization length of the localized state. From equations (3) and (4), the following relationship,

$$\ln\left(\sigma T^{1/2}\right)\alpha T^{-1/4}, \quad (6)$$

can be obtained. One can plot the $ln(\sigma T^{1/2})$ with $T^{-1/4}$ of all $Zn_{1-x}Y_xO$ nanocrystalline films as shown in Fig. 7 to examine the possibility of Mott VRH conduction mechanism. The result illustrates that the experimental data can be fitted well in the low temperature range as shown in Fig. 7 and demonstrates that the Mott VRH process dominates the conduction mechanism at low temperature for all samples.

As a consequence, the resulting conductivity of all samples can be expressed by the combination of thermal activation conduction and Mott VRH conduction. The temperature-dependent conductivity fits the relationship, $ln\sigma\propto T^{-1}$, in the high temperature range indicating the domination of thermal activation conduction and the relationship, $ln(\sigma T^{1/2})\propto T^{-1/4}$, in the low temperature range indicating the domination of Mott VRH conduction.

Conclusions

The ZnO and Y-doped ZnO nanocrystalline films were separately deposited on the glass substrates by sol-gel method for comparison of microstructure, optical properties and carrier transport behavior. XRD patterns show that all samples are found to exhibit the same wurtzite hexagonal structure of group space $P6_3/mc$. FE-SEM images show the grain size and thickness of $Zn_{1-x}Y_xO$ films decreases with the increase of doping of Y. The temperature-dependent resistivity increases with the doping of Y into the $Zn_{1-x}Y_xO$ films. Meanwhile, the resistivity also increases with decreasing temperature indicating a typical semiconductor behavior in the electrical transport property. The resulting conductivity of all $Zn_{1-x}Y_xO$ films can be expressed by the combination of thermal activation conduction and Mott VRH conduction in which thermal activation and VRH conduction dominated in the high and low temperature range, respectively.

Acknowledgment

This work was sponsored by the National Science Council of the Republic of China under the grants NSC101-2221-E-164-004 and NSC101-2221-E-005-014.

References

[1] P.I. Reyes, C.J. Ku, Z. Duan, Y. Lu, A. Solanki, K.B. Lee, Appl. Phys. Lett. 98 (2011) 173702.
[2] V. Chivukula, D. Ciplys, M. Shur, P. Dutta, Appl. Phys. Lett. 96 (2010) 233512.
[3] M. Ahmad, J. Zhu, J. Mater. Chem. 21 (2011) 599.
[4] K.K. Kim, S. Niki, J.Y. Oh, J.O. Song, T.Y. Seong, S.J. Park, J. Appl. Phys. 97 (2005) 066103.
[5] A. Sedky, T.A. El-Brolossy, S.B. Mohamed, J. Phys. Chem. Solids 73 (2012) 505.
[6] S. Öztürk, N. Kılınç, N. Taşaltin, Z.Z. Öztürk, Thin Solid Films 520 (2011) 932.
[7] A. Alias, K. Hazawa, N. Kawashima, H. Fukuda, K. Uesugi, Jpn. J. Appl. Phys. 50 (2011) 01BG05.
[8] N. Hirahara, B. Onwona-Agyeman, M. Nakao, Thin Solid Films 520 (2012) 2123.
[9] N. Yamamoto, T. Yamada, H. Makino, T. Yamamoto, J. Electrochem. Soc. 157 (2010) J13.
[10] Y. Fukuma, K. Goto, S. Senba, S. Miyawaki, H. Asada, T. Koyanagi, and H. Sato, J. Appl. Phys. 103 (2008) 053904.
[11] Y. Niwayama, H. Kura, T. Sato, M. Takahashi, T. Ogawa, Appl. Phys. Lett. 92 (2008) 202502.
[12] W. Yu, L.H. Yang, X.Y. Teng, J.C. Zhang, Z.C. Zhang, L. Zhang, G.S. Fu, J. Appl. Phys. 103 (2008) 093901.
[13] A.P. Palomino, O. P. Perez, R. Singhal, M. Tomar, J. Hwang, P. M. Voyles, J. Appl. Phys. 103 (2008) 07D121.
[14] Z. Yang, J.L. Liu, M. Biasini, W.P. Beyermann, Appl. Phys. Lett. 92 (2008) 042111.
[15] Y.F. Tian, S.S. Yan, Y.P. Zhang, H.Q. Song, G.L. Liu, Y.X. Chen, L.M. Mei, J. Appl. Phys. 100 (2006) 103901.
[16] K. Ueda, H. Tabata, T. Kawai, Appl. Phys. Lett. 79 (2001) 988.
[17] T.S. Herng, S.P. Lau, L. Wang, B.C. Zhao, S.F. Yu, M. Tanemura, A. Akaike, K.S. Teng, Appl. Phys. Lett. 95 (2009) 012505.
[18] X.X. Wei, C. Song, K.W. Geng, F. Zeng, B. He, F. Pan, J. Phys.: Condens. Matter 18 (2006) 7471.
[19] A. Goyal, S. Kachhwaha, Mater. Lett. 68 (2012) 354.
[20] C.-Y. Tsay, H.-C. Cheng, Y.-T. Tung, W.-H. Tuan, C.-K. Lin, Thin Solid Films 517 (2008) 1032.
[21] K.J. Chen , F.Y. Hung , S.J. Chang , Z.S. Huc, Appl. Surf. Sci. 255 (2009) 6308.
[22] A. Eiling, J.S. Schilling, J. Phys. F: Met. Phys. 11 (1981) 623.
[23] J. Han, M. Shen, W. Cao, Appl. Phys. Lett. 82 (2003) 67.
[24] Y. F. Tian, S.-S. Yan, Y. P. Zhang, H. Q. Song, G. Ji, G. L. Liu, Y. X. Chen, L. M. Mei, J. Appl. Phys. 100 (2006) 103901.
[25] S. Majumdar, P. Banerji, J. Appl. Phys. 107 (2010) 063702.
[26] J. Robertson, Phil. Mag. B 63 (1994) 307.
[27] N.M. Ahmed, Z. Sauli, U. Hashim, Y. Al-Douri, Int. J. Nanoelectron. Mater. 2 (2009) 189.
[28] N. F. Mott, J. Non-Cryst. Solids 1 (1968) 1.
[29] M. L. Knotek, M. Pollak, J. Non-Cryst. Solids 8-10 (1972) 505.
[30] A. L. Efros, B. I. Shklovskii, J. Phys. C 8 (1975) L49.
[31] J.-J. Kim, H.J. Lee, Phys. Rev. Lett. 70 (1993) 2798.
[32] R. Kumar, N. Khare, Thin Solid Films 516 (2008) 1302.
[33] G. Paasch, T. Lindner, S. Scheinert, Synth. Met. 132 (2002) 97.